Available online at www.sciencedirect.com
SCIENCE DIRECT
Journal of Nuclear Materials 353 (2006) 27–34
journal of nuclear materials
www.elsevier.com/locate/jnucmat

Small-angle neutron scattering study of post-irradiation annealed neutron irradiated pressure vessel steels

A. Ulbricht [a], F. Bergner [a,*], C.D. Dewhurst [b], A. Heinemann [c]

[a] Forschungszentrum Rossendorf, P.O. Box 510119, 01314 Dresden, Germany
[b] Institut Laue-Langevin, 6 rue Jules Horowitz, BP 156, 38043 Grenoble cedex 9, France
[c] Hahn-Meitner Institut Berlin, Glienicker Strasse 100, 14109 Berlin, Germany

Received 11 November 2005; accepted 3 February 2006

Abstract

Neutron irradiated reactor pressure vessel steels of two different Cu contents exposed to isochronal post-irradiation annealing treatments at stepwise increasing levels of temperature have been investigated. Results of small-angle neutron scattering experiments are reported and compared with the respective unirradiated and as-irradiated conditions. Volume distributions of scatterers and ratios of total-to-nuclear scattering intensities (A-ratio) were calculated from the measured differential macroscopic scattering cross-sections. Finally, total volume fractions of scatterers, peak radii of the volume distribution and partial information on the composition of scatterers were extracted and discussed as a function of Cu level and annealing temperature. Our measurements indicate that irradiation-induced clusters dissolve completely for the lower Cu level of 0.15 wt% but dissolve only partly prior to the onset of coarsening for the higher Cu level of 0.29 wt%. An Arrhenius type behaviour and a remarkable reversibility of the irradiation-induced cluster distribution are observed in the complete dissolution regime.

1. Introduction

Neutron irradiation induces an increase of the brittle-to-ductile transition temperature of reactor pressure vessel (RPV) steels. It is now generally accepted that for low levels of phosphorus this increase is essentially caused by the formation and evolution of nm-sized copper enriched solute clusters [1] and/or (depending on composition) additional features specified as matrix damage [2] or vacancy solute complexes [3]. It is also known that these clusters tend to dissolve for low-Cu (less or about 0.1 wt%) RPV steels during a post-irradiation annealing treatment [4,5] and that the transition temperature shift is (at least partially) reversed [6]. However, the characteristics of the dissolution process are not yet well documented, not to mention mechanistic understanding. Furthermore, the conditions under which complete dissolution switches into coarsening observed at higher Cu concentrations (higher than or about 0.2 wt%) [7–9] are also not clear.

* Corresponding author. Tel.: +49 351 260 3186; fax: +49 351 260 2205.
E-mail address: F.Bergner@fz-rossendorf.de (F. Bergner).

0022-3115/$ - see front matter © 2006 Elsevier B.V. All rights reserved.
doi:10.1016/j.jnucmat.2006.02.083

Among the experimental methods capable of detecting and characterizing irradiation-induced clusters, small-angle neutron scattering (SANS), first applied in [10], is the only technique allowing a statistically representative size distribution of clusters to be calculated [2]. The calculation relies, however, on a number of assumptions, e.g. about composition or the resulting magnetic moment of the clusters [11]. The aim of the present paper is to contribute to the understanding of cluster dissolution by reporting and discussing results of SANS experiments performed after isochronal post-irradiation annealing treatments (annealing time: 10 h) at stepwise increasing levels of temperature.

2. Experiments

The chemical composition of the materials investigated is given in Table 1. The basic compositions correspond to the specification of ASTM A533B cl.1 RPV steel. Materials M1 and M2 provided within the framework of international research programs are also known under the designations JRQ and JPA, respectively. Mechanical properties, product specifications and final heat treatment are summarized in [12]. The microstructure of the low-alloy steels is bainitic–martensitic with a body-centered cubic iron unit cell. Notched bars of dimensions $10 \times 10 \times 55\ \mathrm{mm}^3$ were irradiated in the prototype VVER-2 reactor at a temperature of 528 K (255 °C) up to three different neutron fluences for both materials. The irradiation conditions are summarized in Table 2.

From the irradiated specimens M1-I3 and M2-I2, slices of about 1 mm thickness were cut in order to perform isochronal annealing treatments. The annealing time was 10 h for each slice followed by furnace cooling. The annealing temperatures applied to the individual slices are given in Table 3.

SANS measurements were performed at the spectrometers V4 of HMI-BENSC Berlin [13] and D11 of ILL Grenoble [14]. In order to separate magnetic and nuclear scattering contributions, the specimens were placed in a saturation magnetic field of $B = 1.4\ \mathrm{T}$ perpendicular to the incident neutron beam. The scattering vectors, Q, covered the range from 0.2 to $3.0\ \mathrm{nm}^{-1}$. The absolute calibration was carried out using a water standard [15]. The volume distribution of scatterers defined as differential volume fraction, c_R, of scatterers of size between R and $R + \mathrm{d}R$ was calculated from the magnetic scattering contribution using the indirect transformation method developed by Glatter [16], which solves the inverse problem defined by Eq. (1) for $c_R(R)$.

$$\left(\frac{\mathrm{d}\Sigma}{\mathrm{d}\Omega}\right)_{\mathrm{mag}} = \int \Delta\eta^2_{\mathrm{mag}} c_R(R) V(R) F(Q,R)\,\mathrm{d}R. \qquad (1)$$

In Eq. (1), $(\mathrm{d}\Sigma/\mathrm{d}\Omega)_{\mathrm{mag}}$ is the measured magnetic contribution to the differential macro-scopic scattering cross-section per solid angle, $\Delta\eta^2$ is the magnetic scattering contrast, V is the volume of scatterers and F is the form factor. A two-phase model of uniformly dispersed spherical scatterers of vanishing magnetic moment in the homogeneous matrix of ferromagnetic bcc iron is assumed here. It should be emphasized that the calculated total volume fraction of scatterers does not depend on the shape of the scatterers. Additional information on the composition of the scatterers is obtained on the basis of the A-ratio defined as ratio of total SANS cross-section and the nuclear component. Data analysis is described in more detail in [12].

Table 2
Irradiation conditions (irradiation temperature: 528 K)

Material code	Neutron fluence/10^{18} cm^{-2} ($E > 0.5$ MeV)	Flux density/10^{12} cm^{-2} s^{-1} ($E > 0.5$ MeV)
M1-I1	10	0.15
M1-I2	77	3.0
M1-I3	139	5.4
M2-I1	10	0.15
M2-I2	80	3.1
M2-I3	143	5.5

Table 1
Composition of the materials (analysis) in wt% (balance Fe)

Code	C	Mn	Si	Cr	Ni	Mo	V	S	P	Cu
M1	0.20	1.42	0.23	0.13	0.80	0.52	0.008	0.005	0.020	0.15
M2	0.18	1.33	0.26	0.16	0.73	0.55	0.006	0.004	0.020	0.29

Table 3
Microstructural parameters characterizing the irradiation-induced clusters and effect of annealing

Material/condition	Annealing temperature, T (K)	Volume fraction, c (%)	Peak radius, R_p (nm)	A-ratio	ΔHV10[a]
M1-I1	As-irradiated	0.21 ± 0.01	1.04 ± 0.05	2.1 ± 0.2	58 ± 5
M1-I2	As-irradiated	0.34 ± 0.01	1.00 ± 0.05	2.4 ± 0.2	83 ± 5
M1-I3	As-irradiated	0.50 ± 0.02	1.04 ± 0.05	2.6 ± 0.2	103 ± 5
M1-I3-A1	623	0.48 ± 0.02	1.08 ± 0.05	2.4 ± 0.2	112 ± 5
M1-I3-A2	648	0.46 ± 0.02	1.08 ± 0.05	2.4 ± 0.2	93 ± 5
M1-I3-A3	673	0.39 ± 0.02	1.10 ± 0.05	2.4 ± 0.2	87 ± 5
M1-I3-A4	698	0.29 ± 0.02	1.10 ± 0.05	2.2 ± 0.2	63 ± 5
M1-I3-A5	723	0.06 ± 0.01	1.06 ± 0.05	2.0 ± 0.2	24 ± 5
M1-I3-A6	748	0.02 ± 0.01	1.1 ± 0.1	2.0 ± 0.2	15 ± 5
M2-I1	As-irradiated	0.62 ± 0.03	1.04 ± 0.05	2.7 ± 0.2	87 ± 5
M2-I2	As-irradiated	0.75 ± 0.03	1.16 ± 0.05	2.5 ± 0.1	113 ± 4
M2-I2-A1	623	0.73 ± 0.03	1.08 ± 0.05	2.5 ± 0.1	94 ± 7
M2-I2-A3	673	0.64 ± 0.03	1.10 ± 0.05	2.5 ± 0.1	75 ± 6
M2-I2-A4	698	0.57 ± 0.02	1.14 ± 0.05	2.5 ± 0.1	70 ± 6
M2-I2-A6	748	0.24 ± 0.02	1.25 ± 0.1	4.0 ± 0.2	27 ± 6
M2-I3	As-irradiated	0.83 ± 0.04	1.10 ± 0.05	2.7 ± 0.2	121 ± 5

[a] Unirradiated reference: M1: HV10 = 204 ± 4, M2: HV10 = 222 ± 3.

3. Results

Results of SANS measurements for the as-irradiated conditions of material M1 were reported in [12]. Scattering curves and volume distributions of the unirradiated condition, the as-irradiated condition (M1-I3), and the irradiated and annealed conditions (M1-I3-A3 to M1-I3-A6) are presented in Figs. 1 and 2. The effect of post-irradiation annealing is apparent in both the measured scattering curves and the calculated volume distributions. The scattering curves for the specimens annealed at 623 K and 648 K (conditions M1-I3-A1 and M1-I3-A2) are located between the as-irradiated condition (M1-I3) and the annealing at 673 K (M1-I3-A3). They are not included in Fig. 1 for the sake of clearness. There is no indication for the calculated volume distributions to consist of more than one component (i.e. to be bimodal or multi-modal) for each of the conditions investigated and for the covered size range. In principle, the magnetic and nuclear scattering contributions exhibit the same behaviour. Small differences can be extracted on the basis of the A-ratio (see Table 3).

The magnetic contributions to the scattered intensity and the calculated volume distribution for material M2 are plotted in Figs. 3 and 4, respectively. The behaviour of the materials M1 and M2 is observed to be basically similar.

The microstructural parameters obtained from the SANS experiments are compiled in Table 3.

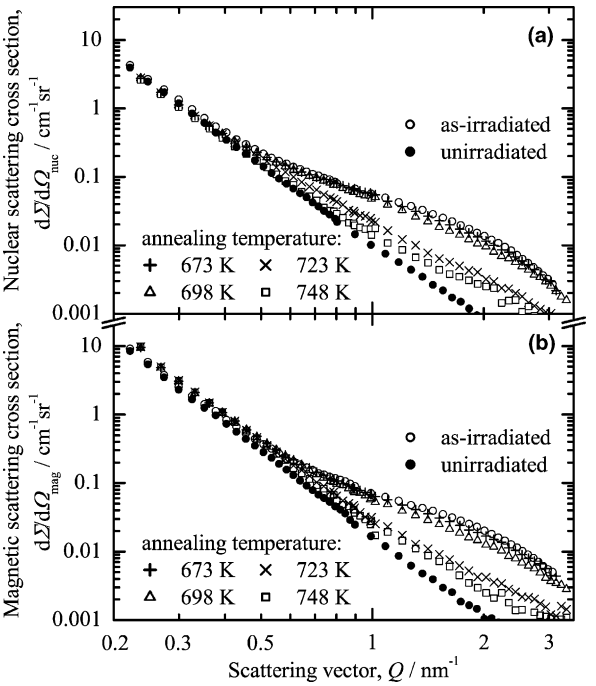

Fig. 1. Nuclear (a) and magnetic (b) scattering cross-section, $d\Sigma/d\Omega$, vs. scattering vector, Q, for the unirradiated condition, M1, the as-irradiated condition, M1-I3, and the annealed conditions, M1-I3-A3 to -A6 of material M1.

The total volume fraction, c, of scatterers was calculated by integrating the volume distribution, $c_R = f(R)$. The radius, R_p, is defined as the peak abscissa of the function, $c_R = f(R)$. Both A-ratio and

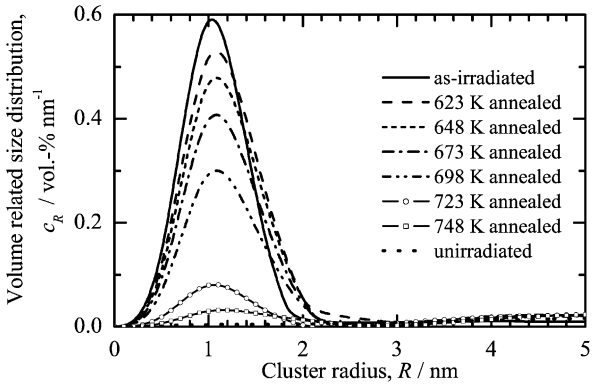

Fig. 2. Volume fraction of scatterers per radius interval, c_R, vs. cluster radius, R, for the unirradiated condition, M1, the as-irradiated condition, M1-I3, and the annealed conditions M1-I3-A1 to -A6.

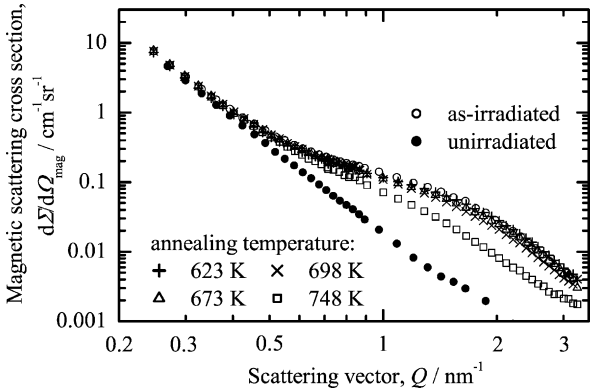

Fig. 3. Magnetic scattering cross-section, $d\Sigma/d\Omega$, vs. scattering vector, Q, for the unirradiated condition, M2, the as-irradiated condition, M2-I2, and the annealed conditions, M2-I2-A1, -A3, -A4 and -A6 of material M2.

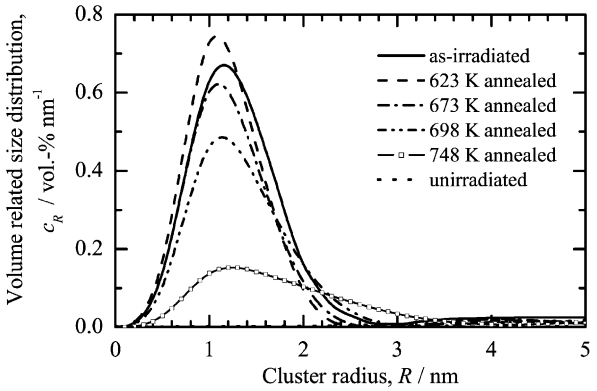

Fig. 4. Volume fraction of scatterers per radius interval, c_R, vs. cluster radius, R, for the unirradiated condition, M2, the as-irradiated condition, M2-I2, and the annealed conditions M2-I2-A1, -A3, -A4 and -A6.

measured hardness difference with respect to the unirradiated condition are also included. The dependence of the total volume fraction of the as-irradiated conditions on neutron fluence is plotted in Fig. 5. The data points for the as-irradiated conditions selected to perform the annealing treatments are marked as full symbols.

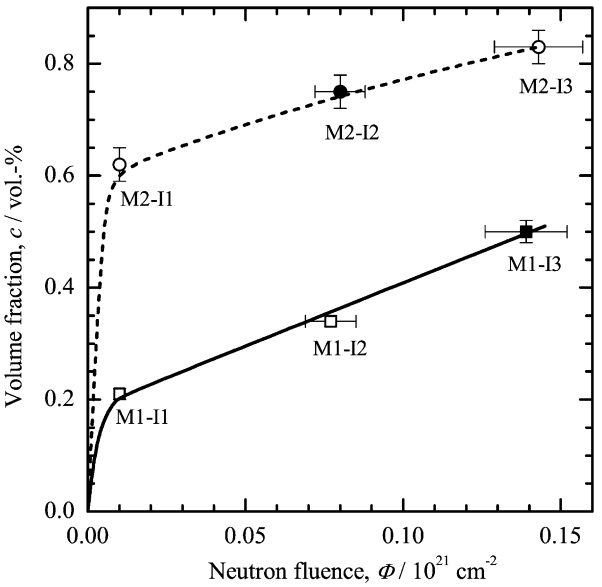

Fig. 5. Total volume fraction of irradiation-induced clusters, c, vs. neutron fluence, Φ, for materials M1 and M2. Irradiation conditions marked by full symbols were subject to annealing treatments.

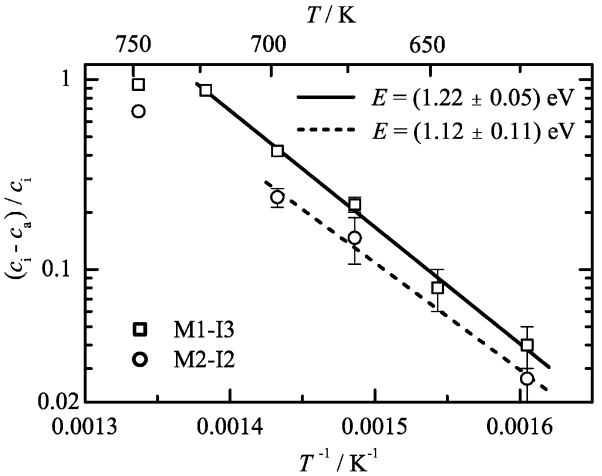

Fig. 6. Arrhenius plot of the dissolved fraction of irradiation-induced clusters, $(c_i - c_a)/c_i$, as a function of the annealing temperature, T, starting from the as-irradiated conditions M1-I3 and M2-I2.

From Figs. 1–4 and Table 3 it is observed that the total volume fraction of irradiation-induced clusters left after 10-h annealing is a decreasing function of the annealing temperature, whereas both peak radius and shape of the volume distribution are essentially constant. The fractional reduction of the total volume fraction of irradiation-induced scatterers, $(c_i - c_a)/c_i$, where c_i and c_a are the total volume fractions in the as-irradiated and annealed condition, respectively, is presented as a function of the inverse absolute annealing temperature, $1/T$, in Fig. 6. With the exception of the highest annealing temperature, the observed dependence can be described by straight lines, the slopes of which are (1.22 ± 0.05) eV for material M1-I3 and (1.12 ± 0.11) eV for material M2-I2.

4. Discussion

The most striking effect of post-irradiation annealing documented in Table 3 is the reduction of the total volume fraction of irradiation-induced clusters with increasing annealing temperature at approximately constant peak radius of the volume distribution (with the exception of the 748 K annealing of material M2-I2, i.e. condition M2-I2-A6). This observation immediately suggests that a certain number of irradiation-induced clusters essentially dissolve. Furthermore, the characteristic dissolution time of a single cluster must be much less than the annealing time of 10 h. Otherwise, i.e. if the characteristic dissolution time were of the same order of magnitude as the annealing time (or even longer than that), the volume distribution would exhibit a shift to lower radii, which is contradictory to observation (Figs. 2 and 4). Pareige et al. [4] have drawn a similar conclusion on the basis of a combined investigation by means of SANS and atom probe field ion microscopy (APFIM) of a neutron-irradiated French RPV steel (0.07 wt% Cu) annealed at 723 K for 2 h, 20 h, and 100 h. These authors estimated the characteristic dissolution time of a single cluster to be less than 2 h at 723 K. From the present investigation it can be concluded that any remainder of the clusters after 'dissolution' must be smaller than the detection limit of SANS, i.e. smaller than 0.5 nm. This conclusion holds analogously for any of the annealing temperatures applied.

According to Pareige et al. [4] the entire process of successive dissolution events of clusters at an annealing temperature of 723 K (450 °C) is not finished after 20 h of annealing. It is assumed that the same situation applies to the present annealing treatments. Therefore, the measured volume distributions represent an intermediate stage (not a final stage or saturation). Nevertheless, the observed Arrhenius like behaviour documented in Fig. 6 strongly suggests that:

(1) The process that controls the frequency of successive dissolution events is a thermally activated process.
(2) The dissolution is controlled by the same process over the entire range of annealing temperatures.
(3) The apparent activation energy, E, given by the magnitude of the slope of the straight lines is about 1.2 eV (Fig. 6).

The calculated ranges of the slope overlap for materials M1 and M2 (Fig. 6). It is therefore reasonable to assume the same process to control the dissolution rate for both materials.

It is important to note that the slope of the straight lines can only be interpreted in terms of a physical activation energy, if the system is in the steady state. In the present case this requires the dissolution process to proceed at a constant rate (independent of time but depending on temperature) over the 10 h of annealing. This requirement is not fulfilled at the highest annealing temperature, $T = 748$ K (Fig. 6), because the dissolution process is obviously completed within a shorter time for material M1 and there is a cross-over from dissolution to growth for material M2. Therefore, the data points obtained for this temperature were excluded from the analysis. For the other annealing temperatures, a constant dissolution rate may be a reasonable approximation, but this was not checked within the present set of experiments.

It is not possible to give a conclusive interpretation of the mechanism of the dissolution process on the basis of the present measurements alone. Nevertheless, it is worth noticing that a similar value of about 1.2 eV was obtained for the binding energy of a vacancy to a Cu-vacancy cluster in iron by means of molecular dynamics calculations [17]. This binding energy turned out to be a slowly varying function of the particular number of vacancies and Cu atoms in the cluster in the range of some 10 Cu atoms and some 10 vacancies, i.e. in the size range of interest here. Another estimation (about 1.3 eV) relevant in the present context was obtained from an Arrhenius plot of the growth rate of interstitial loops in electron-irradiated standard-purity iron

[18]. This value was interpreted in terms of vacancy migration under the condition of deep trapping of vacancies by interstitial carbon. For a detailed discussion and a comparison with other estimates we refer to the literature [18].

The A-ratio can be calculated from the following equation:

$$A = \frac{\Delta\eta_{\mathrm{mag}}^2}{\Delta\eta_{\mathrm{nuc}}^2} + 1 = \frac{\left(\sum_{i\in\mathrm{cluster}} n_i b_{i,\mathrm{mag}} - n_{\mathrm{Fe}} b_{\mathrm{Fe,mag}}\right)^2}{\left(\sum_{i\in\mathrm{cluster}} n_i b_{i,\mathrm{nuc}} - n_{\mathrm{Fe}} b_{\mathrm{Fe,nuc}}\right)^2} + 1, \tag{2}$$

n_{Fe} is the number density of iron atoms in the iron lattice, n_i is the number density of atoms of type i in the cluster, b is the scattering length and the subscripts 'nuc' and 'mag' refer to the nuclear and magnetic contribution, respectively. For a cluster consisting of Cu atoms and/or vacancies on Fe lattice sites, the A-ratio can be expressed as follows:

$$A = \left(\frac{6.0}{7.7v - 9.5}\right)^2 + 1, \tag{3}$$

$v = n_{\mathrm{Cu}}/n_{\mathrm{Fe}}$ is the fraction of Cu atoms in the cluster (pure vacancy cluster: $v = 0$, pure bcc Cu: $v = 1$). The A-ratio of pure vacancy clusters and pure bcc Cu clusters in an iron matrix assumes values of about 1.4 and 12, respectively. Average A-ratios of 1.7 and 5 have been observed for irradiation-induced clusters in Fe-based model alloys with 0.015 wt% Cu and 0.42 wt% Cu, respectively [19]. The corresponding average Cu fractions in idealized model Cu-vacancy complexes are 30 at.% and 84 at.% according to Eq. (3). The dependence on annealing temperature of the average A-ratio measured in this work, if any (with the exception of condition M2-I2-A6 to be discussed later), has to be rated as comparatively weak. A small increase of the average A-ratio with neutron fluence (from 2.1 to 2.6, Table 3) and a reversion of this increase due to annealing (from 2.6 to 2.0) is observed for material M1. The observed A-ratio for material M2 (with the mentioned exception) is essentially constant, $A = 2.5$, and corresponds to a Cu fraction in Cu-vacancy complexes of 60 at.%.

The above observations, i.e. (1) a monomodal volume distribution of irradiation-induced clusters for each irradiation or annealing condition, (2) the general Arrhenius like behaviour, and (3) the low variability of the A-ratio, suggest a single type of clusters present after neutron irradiation and post-irradiation annealing with a more or less uniform composition. This is in some contrast with the view inspired e.g. by Fig. 5, according to which two populations of irradiation-induced clusters seem to form: One related to the fast saturating increase of volume fraction, the other one related to the continuous linear increase afterwards.

The annealing condition M2-I2-A6 (i.e. the highest annealing temperature applied, 748 K) exhibits the only significant deviation from the behaviour discussed so far in a number of items:

(1) The peak radius, R_{p}, of the volume distribution is slightly shifted to higher values. This shift is even more pronounced, if the large-radius tail of the size distribution in Fig. 4 is considered.
(2) The measured A-ratio assumes a significantly higher value of 4.0 as compared to a value of 2.5 observed at lower annealing temperatures (Table 3). The corresponding average Cu fractions in idealized model Cu-vacancy complexes are 78 at.% and 60 at.%, respectively, according to Eq. (3).
(3) The 748 K data point in Fig. 6 deviates from the general Arrhenius behaviour.

The conclusion is that, unlike the behaviour discussed so far, coarsening of Cu-rich precipitates takes place for material M2-I2 at an annealing temperature of 748 K. It cannot be decided, whether this coarsening starts from remaining Cu clusters below the detection limit of SANS (i.e. radius smaller than 0.5 nm) or from solute Cu after complete dissolution of the irradiation-induced clusters, but the first option seems to be more reasonable [4]. Coarsening is commonly observed in Fe alloys with higher Cu contents (higher than or about 0.2 wt%) [7–9]. For material M2-I2 (0.29 wt% Cu) the lowest annealing temperature resulting in significant coarsening is between 698 K and 748 K. For material M1-I3 (0.15 wt% Cu) there is no indication of coarsening up to 748 K. At an annealing temperature of 748 K, the irradiation-induced clusters for material M1-I3 are almost completely dissolved (remainder: about 2 vol.% plus defects below the detection limit of SANS). In contrast, at least one coarse Cu-rich cluster was reconstructed by means of tomographic APFIM for the French RPV steel (0.07 wt% Cu) annealed at a lower temperature of 723 K for 100 h [4], but the concentration of such clusters

was estimated to be extremely low (less than 1 vol.% of the concentration in the as-irradiated condition) [4].

It can be summarized that:

- There is a critical Cu content for the present type of alloy. Irradiation-induced clusters dissolve completely for Cu levels lower than the critical one before any coarsening occurs. For higher Cu levels partial dissolution may occur but coarsening is initiated before dissolution is completed. The critical Cu content (higher than 0.15 wt% but less than 0.29 wt% under the present conditions) is expected to depend slightly on the annealing time applied.
- For Cu levels higher than the critical one, two temperature regimes have to be distinguished. At lower temperatures, only (partial) dissolution but no coarsening occurs. At higher temperatures, there is a competition of dissolution and coarsening. The borderline temperature depends on the Cu level and is affected both by applied annealing time and resolution of the method. Under the present conditions, the borderline temperature is between 698 K and 748 K for a Cu level of 0.29 wt%.

There is a remarkable reversibility in the complete-dissolution regime as observed for material M1. This behaviour can be characterized as follows: Starting from the as-irradiated condition, M1-I3:

- Annealing at 623 K or below leaves the properties (including hardness) of the as-irradiated condition M1-I3 approximately unchanged (Table 3).
- Annealing at 748 K approximately reproduces the unirradiated condition M1.
- Annealing at intermediate temperatures results in property changes along the same path in property space ('property' = volume fraction, A-ratio, hardness) as during annealing but in the reverse direction (Table 3).

In this sense there seems to exist an equivalence relation between neutron fluence and annealing temperature to be specified in ongoing work. In other words, clusters formed first (at the lowest fluence) require the highest temperature to dissolve and vice versa. It is therefore reasonable to assume similar mechanisms for cluster formation and dissolution operating in the reverse direction.

5. Conclusion

(1) Depending on the Cu level of the RPV steel investigated, either 'complete' (as seen by SANS) dissolution of the irradiation-induced clusters or onset of coarsening after incomplete dissolution is observed.
(2) The same thermally activated process controls the rate of successive dissolution events for the materials and conditions investigated. The duration of a single dissolution event is much smaller than the applied annealing time of 10 h.
(3) There is a remarkable reversibility of the irradiation-induced property changes (including volume fraction, composition of clusters and hardness) during annealing in the complete-dissolution regime.

Acknowledgements

This work was supported within the PERFECT European Integrated Project under Contract No. F6O-CT-2003-508840 and by the Bundesministerium für Wirtschaft und Arbeit under Contract No. 1501260.

References

[1] G.R. Odette, Scripta Metall. 17 (1983) 1183.
[2] R.G. Carter, N. Soneda, K. Dohi, J.M. Hyde, C.A. English, W.L. Server, J. Nucl. Mater. 298 (2001) 211.
[3] B.D. Wirth, P. Asoka-Kumar, R.H. Howell, G.R. Odette, P.A. Sterne, MRS Symp. Proc. 650 (2001) R6.5.1.
[4] P. Pareige, P. Auger, S. Welzel, J.-C. Van Duysen, S. Miloudi, in: Effects of Radiation on Materials: 19th Int. Symp., in: M.L. Hamilton, A.S. Kumar, S.T. Rosinski, M.L. Grossbeck (Eds.), ASTM STP 1366, ASTM, West Conshohocken, 2000, p. 435.
[5] A. Ulbricht, J. Böhmert, P. Strunz, C. Dewhurst, M.-H. Mathon, Appl. Phys. A 74 (Suppl.) (2002) S1128.
[6] S.K. Iskander, M.A. Sokolov, R.K. Nanstad, in: Effects of Radiation on Materials: 18th Int. Symp., in: R.K. Nanstad, M.L. Hamilton, F.A. Garner, A.S. Kumar (Eds.), ASTM STP 1325, ASTM, West Conshohocken, 1999, p. 403.
[7] G. Solt, F. Frisius, W.B. Waeber, in: Radiation Embrittlement of Nuclear Reactor Pressure Vessel Steels: An International Review, in: L.E. Steele (Ed.), ASTM STP 1011, ASTM, Philadelphia, 1989, p. 229.
[8] G. Solt, F. Frisius, W.B. Waeber, W. Bührer, in: Effects of Radiation on Materials: 14th Int. Symp., in: N.H. Packan, R.E. Stoller, A.S. Kumar (Eds.), ASTM STP 1046, vol. II, ASTM, Philadelphia, 1990, p. 154.
[9] M.A. Sokolov, S. Spooner, G.R. Odette, B.D. Wirth, G.E. Lucas, in: Effects of Radiation on Materials: 18th Int.

Symp., in: R.K. Nanstad, M.L. Hamilton, F.A. Garner, A.S. Kumar (Eds.), ASTM STP 1325, ASTM, West Conshohocken, 2001, p. 333.
[10] F. Frisius, M. Naraghi, Atomkernenergie 29 (1977) 139.
[11] P. Asoka-Kumar, B.D. Wirth, P.A. Sterne, R.H. Howell, Phil. Mag. Lett. 82 (2002) 609.
[12] A. Ulbricht, J. Böhmert, H.-W. Viehrig, J. ASTM Int. 2 (2005) JAI12385.
[13] U. Keiderling, A. Wiedenmann, Physica B 213&214 (1995) 895.
[14] P. Lindner, R.P. May, P.A. Timmins, Physica B 180&181 (1992) 967.
[15] P. Strunz, J. Saroun, U. Keiderling, A. Wiedenmann, R. Przenioslo, J. Appl. Cryst. 33 (2000) 829.
[16] O. Glatter, J. Appl. Cryst. 13 (1980) 7.
[17] A. Takahashi, N. Soneda, S. Ishino, G. Yagawa, Phys. Rev. B 67 (2003) 024104.
[18] A. Hardouin Duparc, C. Moingeon, N. Smetniansky-de-Grande, A. Barbu, J. Nucl. Mater. 302 (2002) 143.
[19] J. Böhmert, A. Ulbricht, A. Kryukov, Y. Nikolaev, D. Erak, in: Effects of Radiation on Materials: 20th Int. Symp., in: S.T. Rosinski, M.L. Grossbeck, T.R. Allen, A.S. Kumar (Eds.), ASTM STP 1405, ASTM, West Conshohocken, PA, 2001, p. 383.